Experimental visualization of lithium diffusion in Li_xFePO_4

SHIN-ICHI NISHIMURA[1], GENKI KOBAYASHI[1], KENJI OHOYAMA[2], RYOJI KANNO[1], MASATOMO YASHIMA[3] AND ATSUO YAMADA[1]*

[1]Department of Electronic Chemistry, Interdisciplinary Graduate School of Science and Engineering, Tokyo Institute of Technology, 4259 Nagatsuta, Midori, Yokohama 226-8502, Japan

[2]Institute for Materials Research, Tohoku University, Sendai 980-8577, Japan

[3]Department of Materials Science and Engineering, Interdisciplinary Graduate School of Science and Engineering, Tokyo Institute of Technology, 4259 Nagatsuta, Midori, Yokohama 226-8502, Japan

*e-mail: yamada@echem.titech.ac.jp

Chemical energy storage using batteries will become increasingly important for future environmentally friendly ('green') societies. The lithium-ion battery is the most advanced energy storage system, but its application has been limited to portable electronics devices owing to cost and safety issues[1]. State-of-the-art LiFePO4 technology as a new cathode material with surprisingly high charge–discharge rate capability has opened the door for large-scale application of lithium-ion batteries such as in plug-in hybrid vehicles[2–5]. The scientific community has raised the important question of why a facile redox reaction is possible in the insulating material[6–14]. Geometric information on lithium diffusion is essential to understand the facile electrode reaction of Li_xFePO_4 ($0 < x < 1$), but previous approaches have been limited to computational predictions[15,16]. Here, we provide long-awaited experimental evidence for a curved one-dimensional chain for lithium motion. By combining high-temperature powder neutron diffraction and the maximum entropy method, lithium distribution along the [010] direction was clearly visualized.

The present lithium-ion battery technology is based on the reversible intercalation reaction discovered in the early 1980s for both the cathode (Li_xCoO_2: $0 < x < 1$) (ref. 17) and the anode (Li_xC_6: $0 < x < 1$) (ref. 18). This technology is widely used for portable electronic devices because its energy density is much higher than that of any other conventional rechargeable battery system. Since the first commercialization by Sony Corporation in 1991 (ref. 19), the combination of these materials has remained basically unchanged. The specific energy density is now twice as large as that of the first product, which is principally due to technical efforts towards efficient packing of components inside a cell rather than due to material innovations. However, such a development strategy has gradually sacrificed the safety margin and increased the risk of explosive accidents initiated by abrupt oxygen extraction from the charged cathode at elevated temperatures. Reduction in cost has also been restricted by the requirement of a large amount of cobalt in the cathode material. Safety and cost are critical issues and have prevented lithium-ion batteries from being used for large-scale applications[1]. Thus, nickel metal hydride batteries are currently used in hybrid vehicles.

Lithium iron phosphate, Li_xFePO_4 ($0 < x < 1$), proposed by Padhi et al. as a new class of cathode materials in 1997 (ref. 2), has the potential to enable the production of large-scale lithium batteries, which is rapidly becoming a reality. Problems related to cost and safety can be solved with minimum expense to energy density by using abundant iron as a full Fe^{3+}/Fe^{2+} one-electron redox centre and fixing all oxygen atoms within the olivine framework through strong P–O covalent bonds[3]. Early in the development of LiFePO4, a limit for current durability was considered an intrinsic limitation because of its insulating nature, but now very high rate operation is possible through the efficient formation of small particles and/or a conductive carbon network[3–5]. In turn, this has raised considerable technical interest in why such a facile electrochemical reaction is possible by small polarons strongly localized on the iron sites in phase-separated LiFePO4 and FePO4 (ref. 2) during electrochemical reaction.

Previous studies have established (1) the existence of solid solution in Li_xFePO_4 over the entire compositional domain ($0 < x < 1$) at temperatures above 520 K (ref. 6); (2) an incomplete size-dependent miscibility gap at room temperature including a small solid-solution compositional domain at $0 < x < \alpha$ and $1 - \beta < x < 1$ (refs 7–9); (3) coupled motion of lithium ions and electrons with a large activation barrier of about 600–800 meV (refs 10,11); (4) a rate-limiting nucleation and facile growth mechanism with cooperative phase boundary movement along the [100] direction[12,13] with a small activation energy of about 130 meV (ref. 14); and (5) computational derivation of the smallest lithium migration energy along the [010] one-dimensional tunnel with the continuous chain of edge-sharing LiO_6 octahedra[15,16]. Among them, anisotropic atomic-scale lithium diffusion is an essential property because it governs the kinetics and geometry of subsequent phase boundary formation in much larger scale (particle-size scale) on two-phase separation between $Li_\alpha FePO_4$ and $Li_{1-\beta}FePO_4$.

Intuitive expectations based on the polyhedral network in the structure provide two possible continuous lithium pathways as shown in Fig. 1, case 1, a chain of octahedral lithium on 4a sites–face-shared vacant tetrahedral sites–face-shared nearest-neighbour octahedral 4a sites along the [010] direction (Fig. 1a,c); and case 2, a chain of octahedral lithium
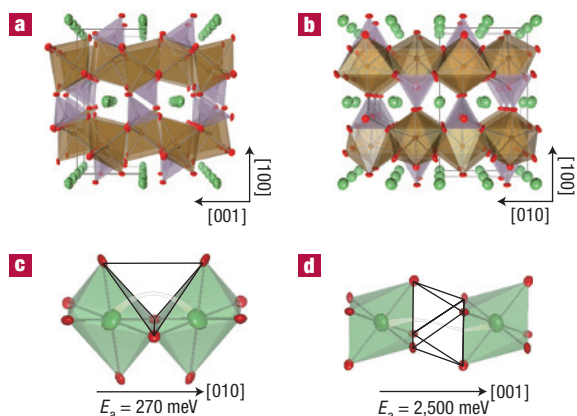
Figure 1 Crystal structure of LiFePO$_4$ and possible lithium pathways. a,b, The crystal structure of LiFePO$_4$ projected along the [010] (**a**) and [001] (**b**) directions. **c,d,** Possible Li diffusion pathways are parallel to these directions. The structures are drawn with the structural parameters obtained through this work and summarized in Supplementary Information, Table S1. The structure can be described as a distorted hexagonal close-packed oxygen sub-array, in which Li, Fe and P atoms occupy interstitial sites to form (1) corner-sharing FeO$_6$ octahedra that are nearly coplanar to form a distorted two-dimensional square lattice perpendicular to the *a* axis, (2) edge-sharing LiO$_6$ octahedra aligned in parallel chains along the *b* axis and (3) tetrahedral PO$_4$ groups connecting neighbouring planes or arrays. The green, brown, purple and red ellipsoids indicate Li, Fe, P and O atoms, respectively. Intuition leads to two possible lithium migration paths: **c**, along the [010] direction through face-shared vacant tetrahedral sites; and **d**, along the [001] direction through face-shared octahedral sites. One-dimensional diffusion along the [010] direction (**c**) was predicted by the computational method[15,16].

on 4*a* sites–face-shared vacant octahedral sites–face-shared second-nearest-neighbour octahedral 4*a* sites along the [001] direction (Fig. 1b,d). The *ab initio* study of Morgan *et al.* using the nudged elastic band method indicated that although Li$^+$ mobility is high in the tunnels along the [010] direction (case 1, Fig. 1c), Li$^+$ hopping between tunnels (case 2, Fig. 1d) is very unlikely[15]. Similar conclusions were reached by Islam *et al.* using empirical potential models[16]. However, no experimental evidence based on direct observation of lithium motion in the atomic scale has been reported.

Neutron diffraction profiles include useful information on lithium, because the scattering ability of the lithium nucleus (amplitude of coherent scattering length) is relatively large and independent of scattering vector $Q = 4\pi \sin\theta/\lambda$. This nature is amenable for detailed analysis of the thermal motion of the lithium nucleus, in contrast to the negligible X-ray scattering ability of lithium or lithium ions with only two or three electrons. To enhance this advantage, ^{7}LiFePO$_4$ was prepared using ^{7}Li-enriched Li$_2$CO$_3$ as the raw material. This greatly improved data quality because the natural existence of 7.5% ^{6}Li causes: (1) about 1.5×10^4 larger absorption; (2) about 15% decrease of coherent scattering length; and (3) larger incoherent scattering. The quality of the sample itself was also confirmed by the high-resolution synchrotron X-ray diffraction profile, and subsequent analysis by the maximum entropy method (MEM). No impurity phase or amorphous hallow was observed and the fit was satisfactory (see Supplementary Information, Fig. S1A). The electron density distribution of LiFePO$_4$ by the MEM is almost identical to that obtained by *ab initio* calculation as shown in Supplementary Information, Fig. S1B.
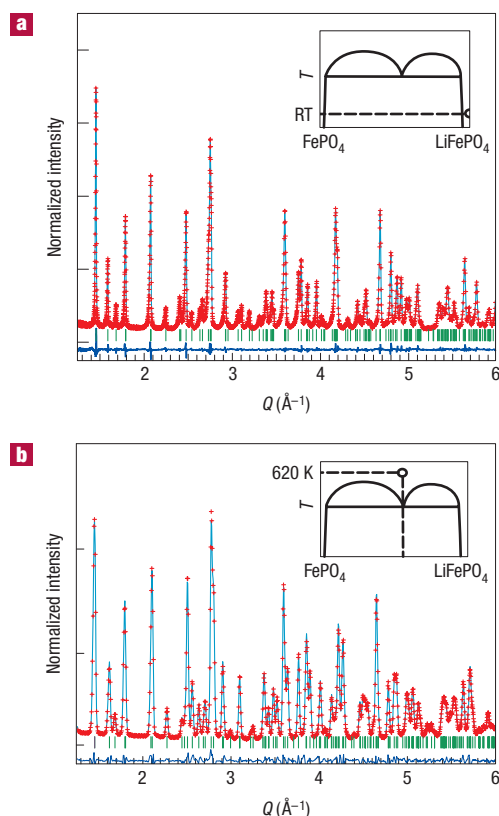

Figure 2 Neutron diffraction patterns measured at two specific points in the FePO$_4$–LiFePO$_4$ binary phase diagram. a,b, Rietveld refinement patterns for the time-of-flight neutron diffraction profile measured for LiFePO$_4$ at room temperature (**a**) and the angle-dispersive neutron diffraction profile measured for Li$_{0.6}$FePO$_4$ at 620 K (**b**). Two different neutron diffractometers were used for different target information for each measurement as explained in the Methods section. The data points are plotted using the common scale $Q = 4\pi\sin\theta/\lambda$ and the common Q range for VEGA and HERMES for comparison. Specific points of measured composition and temperature are given in the inset phase diagram reported by Delacourt *et al.*[6] and Dodd *et al.*[20]. Observed intensity Y_{obs} and calculated intensity Y_{calc} are represented by red plus signs and the green solid line, respectively. The blue curve at the bottom represents the residual difference, $Y_{obs.} - Y_{calc.}$. The refined parameters are summarized in Supplementary Information, Tables S1,S2. No impurity phase was identified, and the crystal structure was successfully refined with the space group *Pnma*.

Figure 2a shows the Rietveld refinement pattern for time-of-flight neutron diffraction data measured at room temperature for ^{7}LiFePO$_4$. Fitting was satisfactory ($R_{wp} = 2.66\%$, $R_F = 0.46\%$, $S = 1.34$) with accurately refined atomic positions as well as anisotropic atomic displacement parameters for all atoms under the classical harmonic oscillation model. Successful measurement and analysis were also carried out for isostructural FePO$_4$. The thermal ellipsoids for Fe, P and O atoms were almost identical for ^{7}LiFePO$_4$ and FePO$_4$ (Supplementary Information, Fig. S2).

Important information is included in the anisotropic atomic displacement parameters for lithium, which determine the overall anisotropy of the thermal vibration by the shape of the ellipsoid. Green ellipsoids shown in Figs 1 and 3 represent the refined lithium vibration. The preferable direction of thermal displacement is towards the face-shared vacant tetrahedra. The expected curved
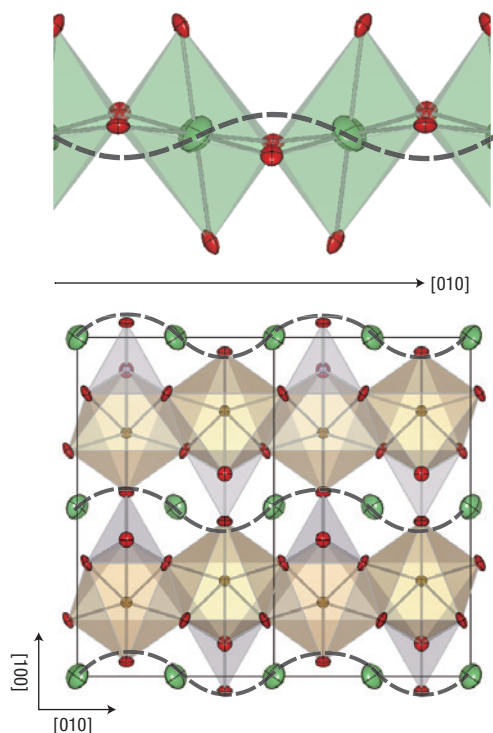
Figure 3 Anisotropic harmonic lithium vibration in LiFePO4 shown as green thermal ellipsoids and the expected diffusion path. The ellipsoids were refined with 95% probability by Rietveld analysis for room-temperature neutron diffraction data. Expected curved one-dimensional continuous chains of lithium motion are drawn as dashed lines to show how the motions of Li atoms evolve from vibrations to diffusion.

one-dimensional continuous chain of lithium atoms is shown in Fig. 3, and is consistent with the computational prediction by Morgan et al.[15] and Islam et al.[16]. Such anisotropic thermal vibrations of lithium were further supported by the Fourier synthesis of the model-independent nuclear distribution of lithium (see Supplementary Information, Fig. S3).

The subsequent experimental direction was significant enhancement of lithium motion by introducing a large number of lithium defects at elevated temperatures to show how the motions of Li atoms evolve from vibrations to diffusion. This was possible with respect to the phase diagram of Li_xFePO_4 reported in the literature, which is shown in the insets in Fig. 2. Delacourt et al.[6] and Dodd et al.[20] confirmed the small miscibility at low temperatures[7,8], but also reported an unusual eutectoid point at about 500 K where the solid-solution phase emerges at approximately $x = 0.6$. At temperatures higher than 570 K, solid solution dominates all compositions. Rapid hopping and delocalization of lithium ions coupled with small polarons were confirmed by motional narrowing of Mössbauer spectra in the solid-solution phases formed at elevated temperatures[11,21].

On the basis of the above binary phase diagram and corresponding lithium dynamics, the composition and temperature of choice for further neutron diffraction study were $x = 0.6$ and $T = 620$ K, as shown in Fig. 2b. A solid-solution phase of $^7Li_{0.6}FePO_4$ was formed simply by mixing the endmembers, $^7LiFePO_4$ and $FePO_4$, in a 6:4 ratio and heating to 620 K in vacuum. A significant difference of the neutron diffraction pattern with that measured at room temperature ($0.6LiFePO_4 + 0.4FePO_4$) is shown

in Supplementary Information, Fig. S4. Temperature-dependent X-ray diffraction profiles were measured in a helium-sealed cell before the neutron diffraction experiment, and confirm the formation of a single phase of compositionally homogeneous $Li_{0.6}FePO_4$ solid solution in the very narrow temperature range of 600–630 K, as shown in Supplementary Information, Fig. S5.

The first analysis carried out for the $Li_{0.6}FePO_4$ solid-solution phase at 620 K was the Rietveld refinement for the neutron diffraction profile and the resultant pattern is summarized in Fig. 2b. The anisotropic displacement parameters were applied for Fe, P and O, but not for Li, because no reliable solution for harmonic vibration of lithium could be found under the localized atom model (see Supplementary Information, Table S2). To evaluate the dynamic disorder of lithium, the MEM was applied to estimate the neutron scattering length density distribution, which corresponds to the nuclear density distribution. The MEM is a model-free method used to calculate precise nuclear densities in solids, including some disorder and/or anharmonic vibrations using experimentally obtained structure factors as an initial input. The MEM is primarily an information-theory-based technique that was first developed by Gull and Daniel[22] in the field of radioastronomy to enhance the information from noisy data. Afterwards, Collins[23] applied its methodology to crystallography for electron density enhancement from X-ray diffraction. In the theory of this methodology, information entropy, which deals with the most probable distribution of numerical quantities over the ensemble of pixels, is considered. Successful MEM enhancement makes it possible to evaluate not only the missing and heavily overlapped reflections but also any type of complicated electron or nuclear distribution, which is hard to describe with the classical structure model. By applying this method, possible bias imposed by the empirical static structural model is reduced, allowing any type of complicated nuclear distribution as long as it satisfies the symmetry requirements. The validity of such a methodology has been well established for plastic crystal[24] and various ionic conductors[25–27].

A three-dimensional contour surface (0.15 fm Å^{-3}) of the nuclear distribution of lithium atoms is shown in Fig. 4. The probability density of lithium nuclei strictly distributes into the continuous curved one-dimensional chain along the [010] direction, which is consistent with the computational predictions by Morgan et al.[15] and Islam et al.[16]. Other atoms, Fe, P and O, remained at their initial positions even after the MEM analysis. Given the two possible diffusion paths in Fig. 1, the microscopic reason for the diffusion anisotropy could be the difference in the electrostatic repulsion, which should be pronounced if there are face-shared polyhedra. Along the [010] direction, whatever the site occupied by the lithium ion during the diffusion process (octahedral 4a site–intermediate tetrahedral vacant site–octahedral 4a site), there is no face sharing with other occupied polyhedra. On the contrary, when the diffusion occurs along the [001] direction, the intermediate octahedral site shares two faces with PO_4 tetrahedra; therefore, the presence of lithium in this octahedral site is very unlikely, leading to a high activation energy. Recall that lithium ions are localized on the initial 4a sites in stoichiometric $LiFePO_4$ at room temperature, but they possess small thermal vibrations along the continuous one-dimensional distribution as shown in Fig. 3. In $Li_{0.6}FePO_4$ at temperatures as high as 620 K, a large number of lithium defects are thermodynamically stabilized, and enough kinetic motional energy is given to each lithium ion to overcome the hopping barrier of the excitonic Li^+–e^- pair[10].

In summary, we applied the MEM to neutron diffraction data for $Li_{0.6}FePO_4$ at 620 K, and successfully visualized the one-dimensional curved lithium diffusion path in Li_xFePO_4. This provides the long-awaited experimental evidence for such
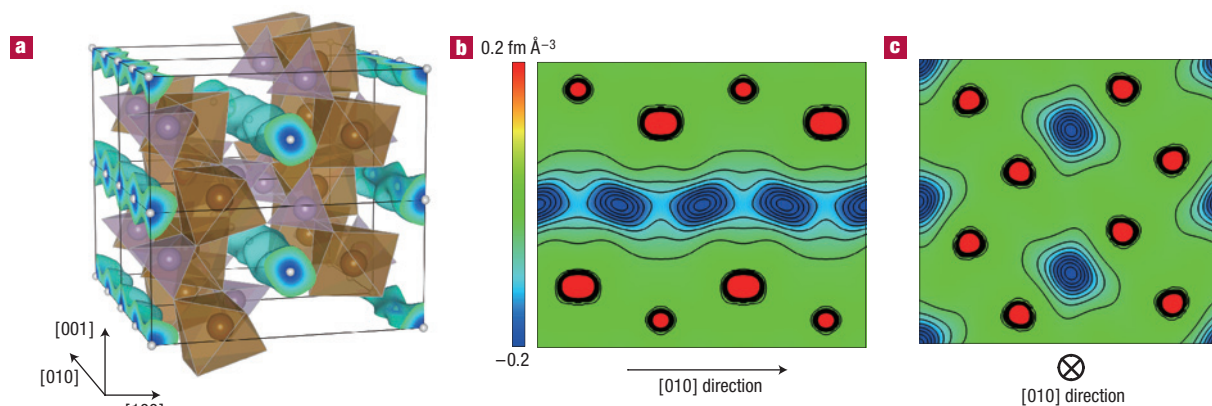
Figure 4 Nuclear distribution of lithium calculated by the MEM using neutron powder diffraction data measured for Li$_{0.6}$FePO$_4$ at 620 K. The classical static atom models with harmonic vibration were no longer appropriate to describe the dynamic disorder of lithium in Li$_{0.6}$FePO$_4$ at 620 K; the MEM nuclear density distribution provided much information on the time and spatially averaged complicated dynamic disorder on lithium diffusion. **a**, Three-dimensional Li nuclear density data shown as blue contours (equi-value 0.15 fm Å^{-3} of the negative portion of the coherent nuclear scattering density distribution). The brown octahedra represent FeO$_6$ and the purple tetrahedra represent PO$_4$ units. **b**, Two-dimensional contour map sliced on the (001) plane at $z = 0.5$; lithium delocalizes along the curved one-dimensional chain along the [010] direction, whereas Fe, P and O remain near their original positions. **c**, Two-dimensional contour map sliced on the (010) plane at $y = 0$; all atoms remain near their original positions.

strong dimensional restriction of lithium motion in Li$_x$FePO$_4$. Beyond Li$_x$FePO$_4$, this is, to our knowledge, the first visual demonstration of the ion diffusion path in a battery electrode. Delocalization of mobile ions at elevated temperatures is a universal phenomena occurring in any intercalation electrode material, and can be used to shed light on the ion dynamics. In particular, such temperature-driven motional enhancement should be more significant in the electron/hole localized system, which has recently been recognized to form an important emerging materials group that may yield new electrode materials. Therefore, high-temperature neutron diffraction coupled with the MEM is a powerful tool for future battery electrode research.

METHODS

SAMPLE PREPARATION

Fine powder of LiFePO$_4$ was prepared by the conventional solid-state reaction method. Lithium carbonate (Wako >99%), iron(II) oxalate dehydrates FeC$_2$O$_4$·2H$_2$O (Aldrich >99%) and diammonium hydrogen phosphate (NH$_4$)$_2$HPO$_4$ were stoichiometrically weighed and thoroughly mixed by high-energy ball milling for 6 h with acetone. This mixture was heated at 700 °C for 6 h under an engineering-grade argon gas flow. For ^{7}LiFePO$_4$, ^{7}Li-enriched Li$_2$CO$_3$ (Toyama Kogyo >99.9%) was used in place of the natural Li$_2$CO$_3$.

FePO$_4$ was prepared by chemical oxidation of LiFePO$_4$ using nitronium tetrafluoroborate NO$_2$BF$_4$ (Aldrich > 95%) as an oxidizing agent. A twofold excess of NO$_2$BF$_4$ was dissolved in acetonitrile before adding the LiFePO$_4$ powder, and stirred for 24 h with purified Ar gas bubbling. The reaction is proposed as follows:

$$LiFePO_4 + NO_2BF_4 \rightarrow FePO_4 + LiBF_4 + NO_2.$$
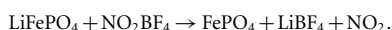
The mixture was filtered and washed several times with acetonitrile before drying the oxidized powder under vacuum.

NEUTRON DIFFRACTION

Two different neutron diffractometers were used with different target information for each measurement: (1) time-of-flight-type VEGA at the High-Energy Accelerator Research Organization (KEK) in Tsukuba Japan, and (2) angle-dispersive-type HERMES, of the Institute for Materials Research

(IMR), Tohoku University, installed in the JRR-3M reactor at the Japan Atomic Energy Agency (JAEA), Tokai, Japan.

For stoichiometric LiFePO$_4$ at room temperature with negligible lithium vacancy and static lithium around the original crystallographic site, the target information was the refined tensor elements β_{ij} of the small thermal harmonic vibration. Data with a large number of separated diffraction peaks measured over the wide range of scattering vector Q ($= 4\pi\sin\theta/\lambda$) are convenient to refine the large number of parameters including β_{ij}. VEGA provides a much wider Q range with higher resolution than HERMES but without data in the very small Q region suitable for MEM analysis (see Supplementary Information, Fig. S6). Time-of-flight neutron powder diffraction data for ^{7}LiFePO$_4$ and FePO$_4$ were collected at room temperature using the backscattering bank of VEGA. The collected data were analysed using the Rietveld method with the RIETAN-2001T computer program modified for VEGA. The Q-dependent incident neutron intensity was considered. The number of reflections included in the range was 4,776 for ^{7}LiFePO$_4$ and 2,245 for FePO$_4$. Peak shape was modelled by a specially designed function for VEGA consisting of the Cole–Windsor function and the pseudo-Voigt function.

For Li$_{0.6}$FePO$_4$ solid solution stabilized at an elevated temperature of 620 K, lithium is in a dynamic state through a large number of its vacancy sites. Much of the information for this widespread lithium ion is in the diffraction peak observed in the region of smaller scattering vector Q, to which HERMES can approach but VEGA cannot. The diffraction peak at the lowest Q for Li$_x$FePO$_4$ is included in this region. Temperature-dependent (room-temperature to 620 K) angle-dispersive neutron powder diffraction data for ^{7}Li$_{0.6}$FePO$_4$ were collected at HERMES. Neutrons with a wavelength of 1.82646(6) Å were obtained by 331 reflection of the Ge monochromator. The fine-powder sample was sealed in a vanadium cylinder, 10 mm in diameter and 70 mm tall, and mounted in the high-temperature chamber. The chamber was evacuated using a turbo pump to avoid sample oxidation. The diffracted beam was detected by a 150 ^{3}He detector system with Cd blades and slits in the 2θ range 5–155° at intervals of 0.1°. The collected data were analysed by the Rietveld method and MEM-based pattern fitting with the computer program RIETAN-2000 and PRIMA (ref. 28). Peak shape was approximated by the split pseudo-Voigt function, and the background profile was approximated with an 8-parameter Legendre polynomial. The unit cell, zero point, background, profile shape and crystal structure parameters were simultaneously refined. The coherent scattering length adopted for Rietveld refinement was −2.22 fm for ^{7}Li, 9.45 fm for Fe, 5.13 fm for P and 5.803 fm for O. The 63 and 214 reflections were used for MEM calculations and Rietveld refinement, respectively. The crystal structure and scattering length

density distribution were analysed and visualized using the computer program VESTA (ref. 29).

References

1. Armand, M. & Tarascon, J. M. Issues and challenges facing rechargeable batteries. *Nature* **414**, 359–367 (2001).
2. Padhi, A. K., Nanjundaswamy, K. S. & Goodenough, J. B. Phospho-olivines as positive-electrode materials for rechargeable lithium batteries. *J. Electrochem. Soc.* **144**, 1188–1194 (1997).
3. Yamada, A., Chung, S. & Hinokuma, K. Optimized LiFePO$_4$ for lithium battery cathodes. *J. Electrochem. Soc.* **148**, A224–A229 (2001).
4. Huang, H., Yin, S.-C. & Nazar, L. F. Approaching theoretical capacity of LiFePO$_4$ at room temperature at high rates. *Electrochem. Solid-State Lett.* **4**, A170–A172 (2001).
5. Chung, S. Y., Bloking, J. T. & Chiang, Y. M. Electronically conductive phospho-olivines as lithium storage electrode. *Nature Mater.* **1**, 123–128 (2002).
6. Delacourt, C., Poizot, P., Tarascon, J. M. & Masquelier, C. The existence of a temperature-driven solid solution in Li$_x$FePO$_4$ for $0 < x < 1$. *Nature Mater.* **4**, 254–260 (2005).
7. Yamada, A., Koizumi, H., Sonoyama, N. & Kanno, R. Phase change in Li$_x$FePO$_4$. *Electrochem. Solid-State Lett.* **8**, A409–A413 (2005).
8. Yamada, A. *et al.* Room-temperature miscibility gap in Li$_x$FePO$_4$. *Nature Mater.* **5**, 357–360 (2006).
9. Meethong, N., Huang, H.-Y. S., Carter, W. C. & Chiang, Y.-M. Size-dependent lithium miscibility gap in nanoscale Li$_{1−x}$FePO$_4$. *Electrochem. Solid-State Lett.* **10**, A134–A138 (2007).
10. Maxisch, T., Zhou, F. & Ceder, G. *Ab initio* study of the migration of small polarons in olivine Li$_x$FePO$_4$ and their association with lithium ions and vacancies. *Phys. Rev. B* **73**, 104301 (2006).
11. Ellis, B., Perry, L. K., Ryan, D. H. & Nazar, L. F. Small polaron hopping in Li$_x$FePO$_4$ solid solutions: Coupled lithium-ion and electron mobility. *J. Am. Chem. Soc.* **128**, 11416–11422 (2006).
12. Chen, G., Song, X. & Richardson, T. J. Electron microscopy study of the LiFePO$_4$ to FePO$_4$ phase transition. *Electrochem. Solid-State Lett.* **9**, A295–A298 (2006).
13. Laffont, L. *et al.* Study of the LiFePO$_4$/FePO$_4$ two-phase system by high-resolution electron energy loss spectroscopy. *Chem. Mater.* **18**, 5520–5529 (2006).
14. Allen, J., Jow, T. & Wolfenstine, J. Kinetic study of the electrochemical FePO$_4$ to LiFePO$_4$ phase transition. *Chem. Mater.* 2108–2111 (2007).
15. Morgan, D., der Ven, A. V. & Ceder, G. Li conductivity in Li$_x$MPO$_4$ (M = Mn, Fe, Co, Ni) olivine materials. *Electrochem. Solid-State Lett.* **7**, A30–A32 (2004).
16. Islam, M., Driscoll, D., Fisher, C. & Slater, P. Atomic-scale investigation of defects, dopants, and lithium transport in the LiFePO$_4$ olivine-type battery material. *Chem. Mater.* **17**, 5085–5092 (2005).
17. Mizushima, K., Jones, P. C., Wiseman, P. J. & Goodenough, J. B. Li$_x$CoO$_2$ ($0 < x < 1$): A new cathode material for batteries of high energy density. *Mater. Res. Bull.* **15**, 783–789 (1980).
18. Yazami, R. & Touzain, P. A reversible graphite-lithium negative electrode for electrochemical generators. *J. Power Sources* **9**, 365–371 (1983).
19. Nagaura, T. & Tozawa, K. Development of rechargeable lithium batteries. II. Lithium ion rechargeable battery. *Prog. Batteries Solar Cells* **9**, 209–217 (1991).
20. Dodd, J., Yazami, R. & Fultz, B. Phase diagram of Li$_x$FePO$_4$. *Electrochem. Solid-State Lett.* **9**, A151–A155 (2006).
21. Dodd, J., Halevy, I. & Fultz, B. Valence fluctuations of ^{57}Fe in disordered Li$_{0.6}$FePO$_4$. *J. Phys. Chem. C* **111**, 1563–1566 (2007).
22. Gull, S. F. & Daniel, G. J. Image reconstruction from incomplete and noisy data. *Nature* **272**, 686–690 (1978).
23. Collins, D. M. Electron density images from imperfect data by iterative entropy maximization. *Nature* **298**, 49–51 (1982).
24. Schotte, K.-D., Schotte, U., Bleif, H.-J. & Papoular, R. Maximum-entropy analysis of the cubic phases of KOH and KOD, NaOH and NaOD. *Acta Crystallogr. A* **51**, 739–746 (1995).
25. Shikanai, F. *et al.* Neutron powder diffraction study on the high-temperature phase of K$_3$H(SeO$_4$)$_2$. *Physica B* **385–386**, 156–159 (2006).
26. Yashima, M., Itoh, M., Inaguma, Y. & Morii, Y. Crystal structure and diffusion path in the fast lithium-ion conductor La$_{0.62}$Li$_{0.16}$TiO$_3$. *J. Am. Chem. Soc.* **127**, 3491–3495 (2005).
27. Yashima, M. *et al.* Conduction path and disorder in the fast oxide-ion conductor (La$_{0.8}$Sr$_{0.2}$)(Ga$_{0.8}$Mg$_{0.15}$Co$_{0.05}$)O$_{2.8}$. *Chem. Phys. Lett.* **380**, 391–396 (2003).
28. Izumi, F. & Ikeda, T. A Rietveld-analysis program RIETAN-98 and its applications to zeolites. *Mater. Sci. Forum* **321–324**, 198–205 (2000).
29. Momma, K. & Izumi, F. VESTA: A three-dimensional visualization system for electronic and structural analysis. *J. Appl. Crystallogr.* **41**, 653–658 (2008).

Supplementary Information accompanies this paper on www.nature.com/naturematerials.

Author contributions

S.N. carried out sample preparation, room-temperature neutron diffraction experiments at VEGA, structure analysis, MEM analysis and all of the related work in supporting information, G.K. carried out sample preparation and the high-temperature neutron diffraction (HT-ND) experiments at HERMES, K.O. set up the equipment for the HT-ND experiments at HERMES, R.K. co-supervised the project, M.Y. supervised the HT-ND experiments at HERMES, A.Y. conceived, supervised and coordinated the whole project. S.N. and A.Y. wrote the manuscript.

Author information

Reprints and permission information is available online at http://npg.nature.com/reprintsandpermissions. Correspondence and requests for materials should be addressed to A.Y.